



RESEARCH LETTER

10.1002/2016GL069967

Key Points:

- Moment versus duration scaling changes when ruptures reach slip zone boundaries and 2-D rupture growth becomes 1-D
- A continuous, bimodal distribution of stress drops and rupture velocities results in fast or slow slip zones
- A single dislocation model explains both fast and slow slip moment versus duration scaling

Supporting Information:

- Supporting Information S1

Correspondence to:

J. Gomberg,
gomberg@usgs.gov

Citation:

Gomberg, J., A. Wech, K. Creager, K. Obara, and D. Agnew (2016), Reconsidering earthquake scaling, *Geophys. Res. Lett.*, 43, doi:10.1002/2016GL069967.

Received 18 APR 2016

Accepted 10 JUN 2016

Accepted article online 15 JUN 2016

Reconsidering earthquake scaling

J. Gomberg¹, A. Wech², K. Creager³, K. Obara⁴, and D. Agnew⁵

¹U.S. Geological Survey, University of Washington, Seattle, Washington, USA, ²U.S. Geological Survey, Anchorage, Alaska, USA, ³Department of Earth and Space Sciences, University of Washington, Seattle, Washington, USA, ⁴Earthquake Research Institute, University of Tokyo, Tokyo, Japan, ⁵IGPP, University of California, San Diego, La Jolla, California, USA

Abstract The relationship (scaling) between scalar moment, M_0 , and duration, T , potentially provides key constraints on the physics governing fault slip. The prevailing interpretation of M_0 - T observations proposes different scaling for fast (earthquakes) and slow (mostly aseismic) slip populations and thus fundamentally different driving mechanisms. We show that a single model of slip events within bounded slip zones may explain nearly all fast and slow slip M_0 - T observations, and both slip populations have a change in scaling, where the slip area growth changes from 2-D when too small to sense the boundaries to 1-D when large enough to be bounded. We present new fast and slow slip M_0 - T observations that sample the change in scaling in each population, which are consistent with our interpretation. We suggest that a continuous but bimodal distribution of slip modes exists and M_0 - T observations alone may not imply a fundamental difference between fast and slow slip.

1. Introduction

Many studies have suggested that measurements of scalar moment, M_0 , and duration, T , are related as $M_0 = K_f T^3$ for “fast” slip events (regular earthquakes) and $M_0 = K_s T$ for “slow” slip events (shallower and steeper trending striped bands in Figure 1, respectively), in which K_f and K_s are proportionality constants [Ide *et al.*, 2007, 2008; Ide, 2014], although some theoretical studies have inferred that M_0 is proportional to T^n in which $1 < n < 3$ [Ide, 2008; Ben-Zion, 2012; Colella *et al.*, 2013; Liu, 2014]. Here slow and fast refer to slip front propagation velocities, either so slow that seismic radiation is too small or long period to be measurable or fast enough that measurable seismic waves radiate. Fast or slow slip tends to be characteristic of particular regions along fault surfaces, often reflecting depth-dependent properties. Numerous models have been proposed to explain these different M_0 - T scaling relations [Ide, 2008; Ben-Zion, 2012; Colella *et al.*, 2013; Liu, 2014].

Here we show that a single, simple dislocation model of slip events within bounded slip zones [Aki, 1972; Scholz, 1982] explains nearly all M_0 - T observations. As in many other studies we envision zones (Figure 2) where fast slip and slow slip occur. However, rather than requiring different scalings for fast and slow populations as in prevailing interpretations [Ide *et al.*, 2007; Ide, 2008; Ide *et al.*, 2008; Gao *et al.*, 2012] (striped bands in Figure 1), our proposed dislocation model predicts the same change in scaling within each population, from M_0 proportional to T^3 and then to T , when slipping areas reach the boundaries of the slip zone and change from unbounded, 2-D, to bounded, 1-D, growth (solid dark bands in Figure 1). This simple model has been invoked to explain scale changes in these and other parameters for fast earthquakes [Shimazaki, 1986; Romanowicz, 1994; Uchide and Ide, 2010; Scholz, 1982; Shaw, 2013; Pacheco *et al.*, 1992]. We propose that it also applies to slow slip events and importantly explains M_0 - T scaling observations. The inference that the same physics may govern the full spectrum of slip modes derives support from the recent laboratory study of Leeman *et al.* [2016], in which they observed the full spectrum of fast seismic to slow silent slip events, by varying only the effective frictional properties.

As in many other studies we envision a highly simplified fault surface, which to first order may be divided into zones where dominantly fast slip and slow slip occur. Figure 2 conveys one model that is consistent with this vision, proposed by Ando *et al.* [2010], Nakata *et al.* [2011], Ando *et al.* [2012], and Ide [2014]. Leeman *et al.* [2016] suggested that the full spectrum of slip modes may be attributed to variations in frictional properties and behaviors predicted by a 1-D frictional spring-slider model. In the Earth, undoubtedly, these properties are described by broad distributions, and alternative models may be viable. For example, Segall *et al.* [2010] and others proposed that slow slip results when dilatancy strengthening quenches accelerating slip (although some laboratory experiments show that fault gouge compacts during rapid slip [Johnson *et al.*, 2016]).

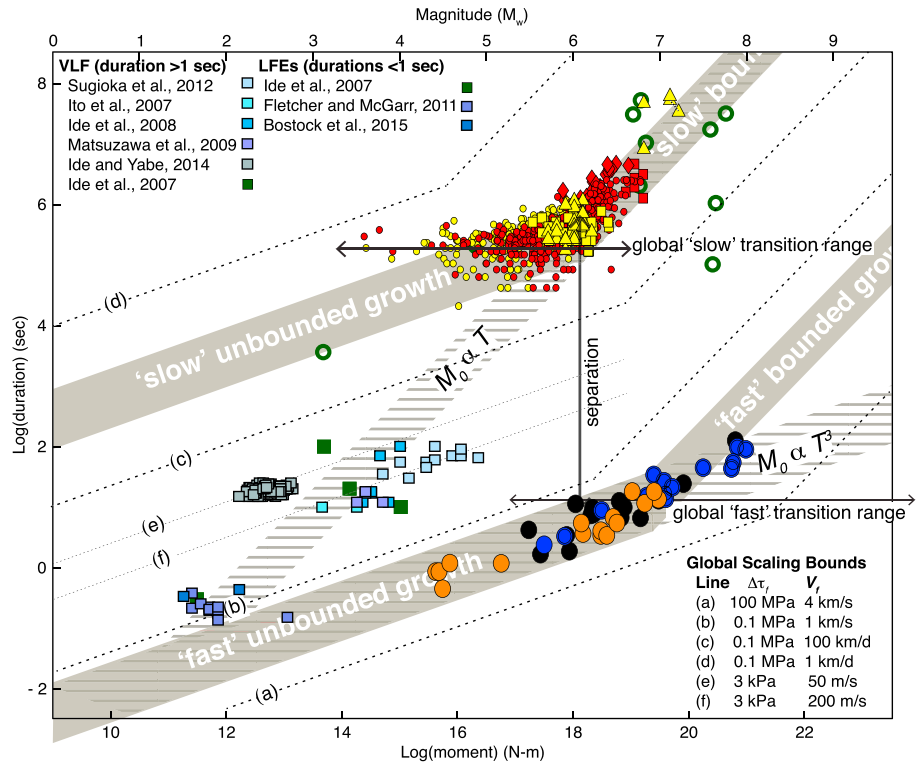


Figure 1. Slip event scalar moment, M_0 , versus duration, T , observations and scaling relationships. The scaling inferred in the study of *Ide et al.* [2007] is shown as lines with horizontal grey stripes, with their observations shown as solid and open dark green symbols indicating seismic and geodetic measurements of fast and slow slip events, respectively. Darker solid grey bands are centered on scaling relations predicted for a dislocation model for a rectangular fault, for populations of slow and fast events and transitions from unbounded to bounded scaling, with thicknesses corresponding to the range of controlling parameters appropriate to the observations made in this study; dashed lines on either side of these two bands show approximate ranges for global observations (a–d in the lower right legend). The vertical double-sided arrow indicates the model-predicted separation between the peaks of the distributions of fast and slow event observations, and horizontal arrows show global scaling transition ranges (see text). Crustal earthquake measurements from different geographic regions are denoted by solid blue, orange, black, and purple circles (see Figure 4). Slow slip observations include our new measurements for Japan and Cascadia shown as solid yellow and red circles, respectively (see Figure 3). Published geodetic measurements of larger slow slip events are shown as squares, triangles, and diamonds for Japan in yellow and Cascadia in red, with different shapes indicating different studies (see Figure 3). Published VLF and LFE measurements are shown as colored squares with references noted in the upper left legend. Dotted lines through these measurements correspond to unbounded scaling, small stress drops, and slow but still seismically observable rupture velocities (e–f in the lower right legend; see text).

Most data sets for the fast population are dominated by events in the unbounded regime, because most big earthquakes occur in subduction zones, where the widths of the seismogenic zones vary from tens to hundreds of kilometers. To resolve the transition from bounded to unbounded regimes, we examined published measurements of continental crustal earthquakes only, where the seismogenic zone typically is less than ~ 30 km. Data for slow events have come mostly from the bounded growth regime, because most geodetic instruments suited to measuring moment can resolve only the larger events. Seismic observations of slow earthquakes have been made in the unbounded region (shown in Figure 1), but we question what constraint they provide on scaling and demonstrate below that they do not rule out our proposed, simpler model. We sample the transition to unbounded slip from the bounded regime using new slow slip measurements that extend the range of observations to smaller, shorter-duration events. Our observations avoid extrapolation across large observational gaps and are limited to southwestern Japan and Cascadia to reduce the natural variability. We find that the scaling of M_0 - T observations for both slow slip and fast slip events, spanning 12 orders of magnitude in M_0 , is consistent with the predictions of the same dislocation theory.

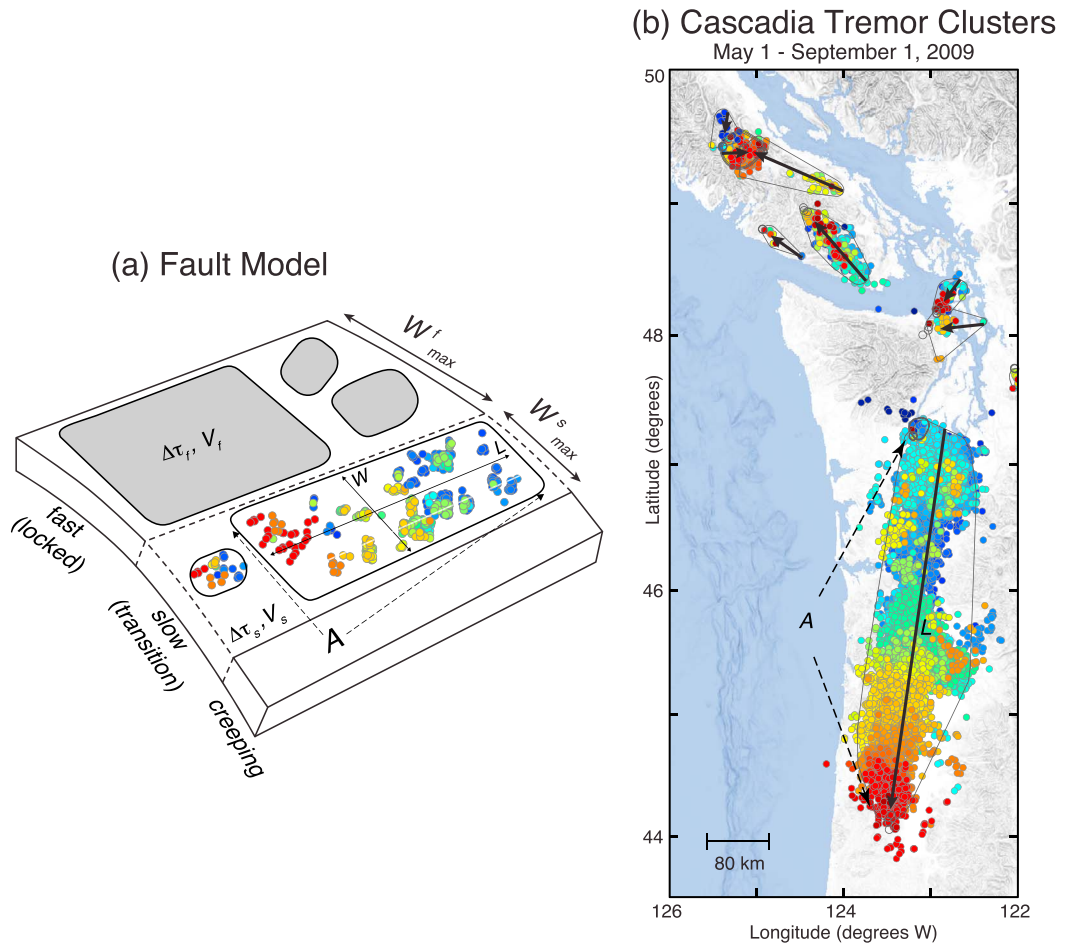


Figure 2. Slip zone fault model and Cascadia slow slip events. (a) Modified subduction zone slip zones [Ito et al., 2007; Ide, 2014]. To first order, the entire fault zone is composed of a velocity strengthening or viscous background (white) with velocity-weakening patches (solid grey and colored areas) having fracture energies that increase with patch size [Ide, 2014]. In the fast zone, with width W_{max}^f , large patches (grey rectangles with length L and width W) slip with high stress drops, $\Delta\tau_f$, at dynamic velocities, V_f , and elasticity dominates. The slow slip zone has width W_{max}^s , contains only clusters of tiny fast patches (colored circles) that permit pulse-like transient slow slip to propagate across the entire surface with low stress drop, $\Delta\tau_s$, and propagation velocity V_s . The patches fail dynamically, triggered as the slow slip front propagates across them, radiating LFEs and tremor signals (colors indicate relative failure time, from blue to red). L is the longest dimension of the slip event and corresponds to the propagation direction. (b) Example of slow slip event dimensions A and L , measured from tremor clusters (see supporting information).

2. Model of Moment Versus Duration Scaling

For simplicity and to describe the theory, as in many studies [Scholz, 1982; Shaw, 2013] we consider slip events with rectangular area, $A=LW$, with length, L , and width W (Figure 2). We measured L as the longest dimension of the slip event and assumed that it corresponds to the propagation direction, so the propagation velocity is $V=L/T$; we verified this assumption for both Japan and Cascadia (see supporting information). The narrowest and constraining boundary of the slip zone is at $W=W_{max}$. As originally proposed by Scholz [1982], when $W < W_{max}$, a slip event grows in two dimensions but when $W=W_{max}$, it can no longer grow in this direction and growth becomes 1-D. We refer to slip events with dimensions $L < W_{max}$ and $L > W_{max}$ as unbounded or bounded, respectively.

Dislocation theory provides a first-order description of fault slip events, beginning with the definition of scalar moment, M_0

$$M_0 = \mu d A \tag{1}$$

d is the average displacement and μ is the rigidity, which dislocation theory relates to the stress drop, $\Delta\tau$ and μ ,

and the fault geometry [Aki, 1972]. We assume a rectangular, buried, dip-slip fault because this is the geometry expected for the most common slow slip events found in subduction zones. The stress drop is then

$$\Delta\tau = c^{-1}\mu d/W \quad (2)$$

where c equals $3\pi/16$. When $\Delta\tau$ is constant, expression (2) describes a “ W model” [Scholz, 1982]. Combining the above definitions, the relationship between M_0 and $\Delta\tau$ becomes

$$M_0 = c\Delta\tau W^2L \quad (3)$$

For unbounded growth both the length and width grow, such that $W=L$. Recalling that $V=L/T$, we rewrite expression (3) as

$$M_0 = c\Delta\tau L^3 = K_u T^3, \quad K_u = c\Delta\tau V^3 \quad (4a)$$

For bounded growth $W=W_{\max}$ and expression (3) becomes

$$M_0 = cW_{\max}^2\Delta\tau L = K_b T, \quad K_b = cW_{\max}^2\Delta\tau V \quad (4b)$$

The result is unbounded and bounded relations identical to those previously attributed to slow and fast slip and inferred to imply fundamentally different slip processes [Ide et al., 2007]. However, rather than K_f describing the entire fast slip population and K_s the slow slip population, each population is described by K_u when events are unbounded and K_b when bounded. The values of K_u and K_b are determined by the distribution of $\Delta\tau$ and V that distinguish each population. The above formulation shows that instead of M_0 - T scaling of fast and slow events implying different underlying physics, all the first-order features of M_0 - T scaling for both populations may be predicted by common dislocation theory and the distributions of just a few parameters that characterize each population.

Observationally, M_0 - T scaling is inferred from $\log(T)$ versus $\log(M_0)$ observations, so that expressions (4a) and (4b) imply that two line segments describe the scaling for each of the fast and slow populations, written

$$\begin{aligned} \log(T) &= 1/3 \log(M_0) - 1/3 \log(K_u), \quad K_u = c\Delta\tau V^3 \quad \text{for } M_0 < c\Delta\tau W_{\max}^3 \\ &= \log(M_0) - \log(K_b), \quad K_b = c\Delta\tau W_{\max}^2 V \quad \text{for } M_0 > c\Delta\tau W_{\max}^3 \end{aligned} \quad (5)$$

Notably, the scaling, or slope of the relationship between $\log(T)$ and $\log(M_0)$, is independent of $\Delta\tau$, V , and W_{\max} and whether slip is fast or slow. Only the value of M_0 where the scaling transition occurs and the intercepts, set by K_u and K_b , differ for each population. These are determined by the values of $\Delta\tau$, V , and W_{\max} that characterize fast slip or slow slip. Additionally, expression (5) predicts the offset between the slow and fast populations: $-(1/3)\log(K_u^5/K_b^3)$.

3. Application to Slow Slip and Fast Slip

The key parameters, $\Delta\tau$, V , and W_{\max} , come from a continuum of states, described by a distribution with one peak characterizing fast slip and another describing slow slip. The widths of the distribution around each peak reflect parameter variability and measurement uncertainty, and although these widths span several orders of magnitude, the separations between fast and slow peaks are even greater. From the literature for fast events globally, parameters span approximate ranges of $W_{\max} \sim 10$ to 200 km, $V_f \sim 1000$ to 4000 m/s [Ito et al., 2007; Schmidt and Gao, 2010; Houston et al., 2011; Kanamori and Brodsky, 2004; Allmann and Shearer, 2009], and $\Delta\tau_f \sim 0.1$ to 100 MPa [Aki, 1972; Kanamori and Brodsky, 2004; Allmann and Shearer, 2009; Shaw, 2013], respectively. For slow events globally, ranges include $W_{\max} \sim 10$ –50 km, $V_s \sim 0.01$ to 1 m/s ~ 1 to 100 km/d [Ito et al., 2007; Schmidt and Gao, 2010; Houston et al., 2011], and $\Delta\tau_s \sim 0.1$ to 100 kPa [Aki, 1972; Kanamori and Brodsky, 2004; Allmann and Shearer, 2009; Shaw, 2013]. Thus, propagation velocities differ by 4 orders of magnitude and stress drops by 3. In Figure 1 we show that the fast and slow predictions differ resolvably, by plotting the scaling relations (expression (5)) predicted for the range of global parameters that yield the minimum and maximum values of K_u and K_b and a transition that assumes $W_{\max} = 40$ km. Figure 1 also shows that a transition may be unresolved in studies that combine global observations, because the global range of W_{\max} corresponds to enormous ranges of predicted transitions, which depend on the cube of W_{\max} [Ide et al., 2007; Peng and Gomberg, 2010; Gao et al., 2012; Liu, 2014].

Parameter ranges are narrower in a single region. Approximate average values appropriate for the observations we have made, for slow slip in southwestern Japan and Cascadia and crustal earthquakes globally, are $\Delta\tau_s = 20$ kPa, $V_s = 10$ km/d, and $W_{\max}^s = 40$ km and $\Delta\tau_f = 1$ MPa, $V_f = 2.5$ km/s, and $W_{\max}^f = 30$ km. In Figure 1 we also plot the relations for these values at the centers of bands with widths equal to one unit in $\log(T)$. In the unbounded region this width corresponds to variation in V or $\Delta\tau$ of 1 or 3 orders of magnitude, respectively. For reasons noted in the next paragraph, we disregard the published observations of low-frequency and very low frequency earthquakes or LFEs and VLFs (squares in Figure 1). The model predictions (segment slopes, transitions, and offset between fast and slow scalings) appear consistent with the remaining observations and allow for the likely variability in stress drop, propagation velocity, and slip zone width.

LFEs and VLFs have been identified in seismic data and interpreted to be slow slip events distinguished by their passbands of about 1–10 Hz or 0.005–0.05 Hz, respectively. We note that the conventional slow M_0 proportional to T scaling is inconsistent with published VLF measurements, even considering only those from a single region. For example, *Ide et al.* [2008] measured M_0 proportional to $T^{3/2}$ but dismissed this deviation from the conventional scaling as an “artifact of the limited frequency range of our analysis, 0.005–0.05 Hz.” Later *Ide* [2008] suggested that M_0 is proportional to T^2 and proposed a different model than that in *Ide et al.* [2007]. Figure 1 shows published VLF measurements from Nankai, Japan, which may be explained by unbounded scaling on a fault characterized by low stress drops and slow, but still seismic, rupture propagation velocities (e.g., dotted lines (e) and (f) in Figure 1 use values reported in *Matsuzawa et al.* [2009]), whether considering measurements from an individual or multiple studies combined. However, despite this consistency, we do not believe that the VLF observations robustly test any scaling or physical model, as the interpretation of VLF sources also is nonunique; i.e., VLFs may radiate from single, coherent slip events or be the result of narrowband filtering of clustered independent LFE arrivals (*J. Gomberg et al.*, Alternative source models of very low frequency events, submitted to *Journal of Geophysical Research Solid Earth*, 2016). We also show LFE measurements from California, Japan, and Cascadia in Figure 1 and suggest that they too may be consistent with low stress drop, slow but seismic propagation velocities, particularly given the small range of moments and large measurement uncertainties associated with such small events. The one study that explicitly focused on assessing LFE scaling found a much weaker dependence of T on M_0 than even for fast earthquakes and concluded that LFEs may differ fundamentally from larger, geodetically observed slow slip events [*Bostock et al.*, 2015]. We concur with this possibility, although confirmation requires additional studies. Finally, we suggest that the extrapolation across the observational gap of many orders of magnitude, between geodetically observed slow slip events and VLFs and LFEs, required to infer the conventional slow slip scaling, seems highly speculative.

Corroboration of the proposed model requires observations that sample the predicted scale changes, without the need to extrapolate across large observational gaps and for which parameters affecting the scaling are drawn from the same population (e.g., come from the same tectonic region). Nearly all previous M_0 - T slow slip observations sampled only the bounded growth regime, being measured using GPS that has a detection threshold for most subduction zone events of $M_w \sim 6$ [*Chapman and Melbourne*, 2009; *Schmidt and Gao*, 2010] and of $M_w \sim 5.4$ in Japan using data from a dense tiltmeter network [*Sekine et al.*, 2010]. Thus, we extend the slow observations across the transition between unbounded and bounded growth expected for Cascadia and Japan (red and yellow symbols, respectively, Figure 1), using measurements of tremor clusters as proxies for slow slip events. Earthquake observations extend well below the expected transition range for fast events. However, we hypothesize that combining global observations blurs transitions, particularly because global earthquake data sets tend to be dominated by subduction zone events with highly variable and large values of W_{\max} . To test this, we carefully examined published estimates of L , W , M_0 , and T , compiled from slip models and parameters in the global database SRCMOD [*Mai and Thingbaijam*, 2014], separating earthquakes for which the expected transition occurs within a measurably small range and well below the largest events (i.e., only crustal events with $W_{\max} < \sim 30$ km).

3.1. Slow Slip Observations

We extend the slow slip M_0 - T population to smaller events using tremor catalogs from Japan [*Obara et al.*, 2010] and Cascadia [*Wech et al.*, 2010] by measuring A , L , and T , corresponding to the area enclosed, the length of the first principal component of the tremor locations, and the interval between the first and last tremors of each cluster (see the supporting information). Previous studies have calibrated the time that tremor is active, or the numbers of tremor events during a cluster to geodetically estimated M_0 values, and used this to

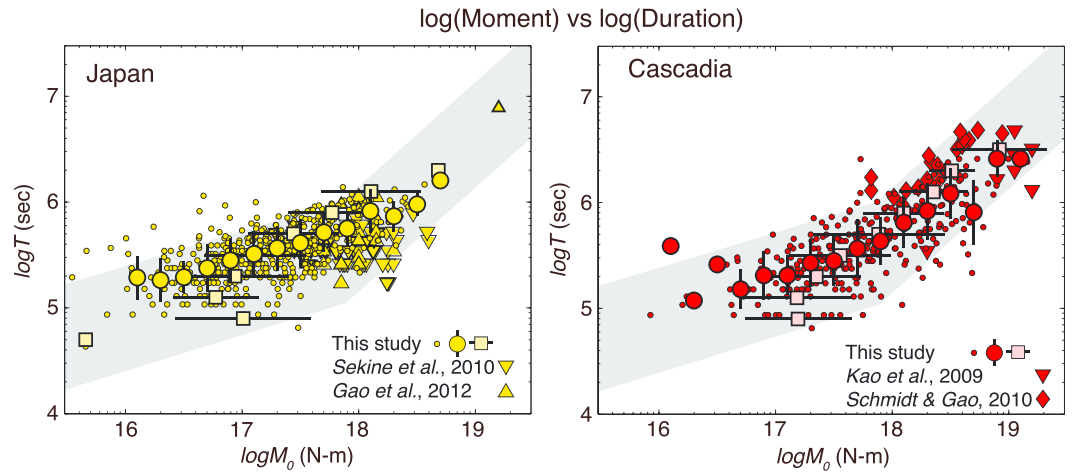


Figure 3. Slow slip M_0 - T measurements. Small circles denote individual measurements made from tremor clusters, and larger circles (darker color) and squares (lighter color) are median values for $\log(M_0)$ and $\log(T)$ bins, respectively, with lines through these denoting RMS deviations from the medians for bins with >2 measurements. Triangles and diamonds are published geodetic measurements of slow slip events in the same regions as the tremor (see legends; squares in Figure 1 shown as inverted triangles). Diagonal bands are the same as those in Figure 1. Tremor cluster M_0 estimates have been corrected for location bias, and durations, T , correspond to the full cluster duration.

estimate M_0 from tremor clusters for inferred slow slip events that are too small for geodetic detection [Aguar *et al.*, 2009; Obara, 2010; Wech *et al.*, 2010]. We took a similar approach but instead calibrated geodetic M_0 versus measurements of $W^2L = A^2/L$, representing the geometric contribution to M_0 , so that the proportionality constant corresponds to an average value of $\Delta\tau$ (equation (3)). Figure S2 shows that our approach yields a slightly better fit to the geodetic M_0 than using tremor numbers [Obara, 2010]. As in previous studies, fit parameters describe the average properties of distributions, and thus, the stress drops we estimate represent measures of the approximate center of a range of $\Delta\tau$ values. For the Japan tremor analysis we constrain the stress drops so that the moments from the tremor clusters match those from 43 published, geodetically estimated, slow slip event moments and durations published in Sekine *et al.* [2010], resulting in $\Delta\tau \sim 30$ kPa. We also show other geodetic estimates from the same region, reported in Gao *et al.* [2012] and listed in Table S1. For Cascadia, a stress drop of $\Delta\tau \sim 10$ kPa yields M_0 - T tremor cluster estimates that are consistent with published geodetic measurements of slow slip events in Kao *et al.* [2009] and Schmidt and Gao [2010]. Figure 3 displays our results for the two regions; while the scatter is substantial, estimates are consistent with the hypothesized scale change. For completeness we show that the hypothesized geometric change in slip event growth from 1-D to 2-D appears consistent with our A and L measurements, which is independent of assumed stress drops or event durations (Figure S3). Because assumptions about how the tremor tracks the slow slip affect duration measurements, we also describe and show M_0 versus two other measures of duration in the supporting information (Figure S1).

3.2. Fast Slip Observations

For the fast slip population, we hypothesized that the transition from bounded to unbounded should be apparent for crustal earthquake measurements, for which the range of W_{\max} should be ~ 10 to 30 km, but would become obscured when measurements from many regions are combined, particularly from convergent margin zones where W_{\max} may vary by hundreds of kilometers (recalling that the transition depends on W_{\max}^3). The existence of this scale change for earthquakes, and its relationship to W_{\max} and other model parameters, has been discussed for over 30 years [Scholz, 1982; Shaw, 2013]. The model we present is the W model, and the L model differs by assuming that the slip is proportional to L instead of W (W is replaced by L in equation (2), for a constant stress drop) and when bounded, M_0 scales as T^2 or L^2 . Indeed, it is difficult to distinguish observationally between an L model and a W model, but again, both models predict a scale change and the observations appear to require one (Figure 4). Other scaling studies find no geometric scale change, suggesting that M_0 is proportional to L^3 even for events with $M_0 > 10^{21}$ N m ($M_w > 8$) [Tanioka and Ruff, 1997; Houston, 2001]; in the supporting information we show that this likely results from combining observations

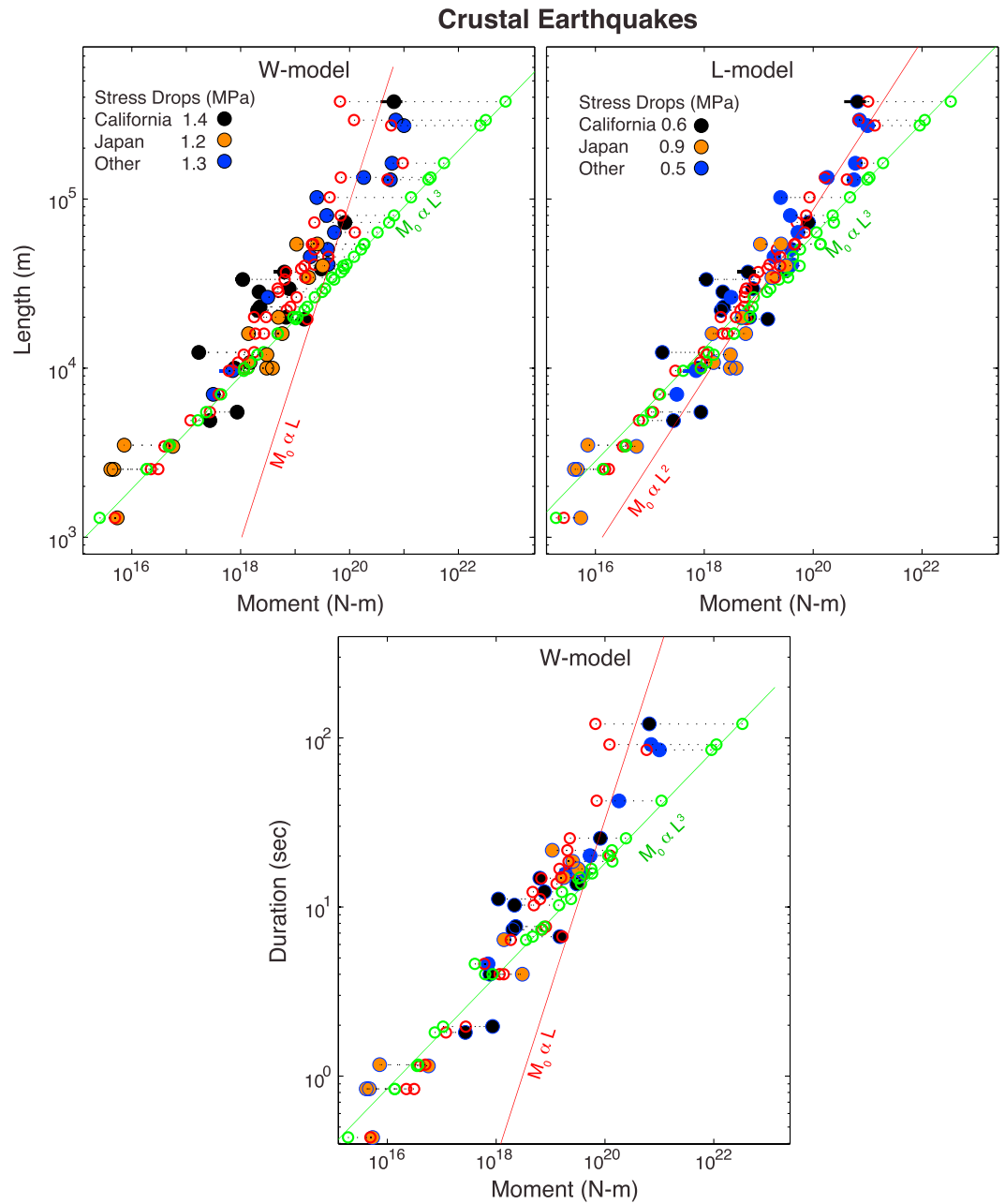


Figure 4. Measured and model-predicted lengths or durations versus M_0 estimates for $M_w > 4$ earthquakes. Estimates of M_0 and L derived from slip models in the SRCMOD database [Mai and Thingbaijam, 2014] (solid circles) connected by dotted lines with corresponding values (open red circles) predicted for bounded (top left) W model or (top right) L model and for an unbounded model (green open circles, all panels). Error bars are standard deviations calculated for earthquakes with >2 entries in the SRCMOD database. Measurements for crustal earthquakes, grouped by tectonic region with stress drops used in model-predicted values that equal the mean difference between the geometric moment and measured M_0 (in legend). Estimates of M_0 versus L , derived from the slip models (Figure 4, top row) and versus (bottom) durations calculated as L/V for earthquakes with database estimates of rupture propagation velocity, V . Red lines have slopes appropriate to bounded W or L models and green lines to unbounded models, to visualize fits between models and data and identification of scale changes.

from many regions, most of which were subduction zones where W_{max} may vary by an order of magnitude or more. As hypothesized and consistent with several previous studies [Romanowicz, 1994; Uchide and Ide, 2010], the crustal earthquake observations clearly require a scale change (Figure 4), although they do not distinguish between a W or L model.

4. Conclusions

Our interpretation of the M_0 - T observations relies only on a dislocation model of slipping faults within bounded fast or slow slip zones, with each zone characterized by just three average parameters: W_{\max} , $\Delta\tau$, and V . While this single simple model explains both fast and slow M_0 - T scaling, knowledge of what controls this distribution is the key to understanding the physics that determine whether fault slip is fast or slow. The remarkable simplicity of our interpretation partly stems from the low-resolution, logarithmic-scale view of the observations and because of observational gaps. Nonetheless, our interpretation allows for a continuous distribution of slip modes but suggests that it may be bimodal with broad peaks diagnostic of fast or slow modes. Recent models explain this, proposing that faults are characterized by only two rheologies, with elastic, velocity-weakening patches exhibiting fast slip embedded in a viscous, velocity-strengthening, background that slips slowly [Ando *et al.*, 2010; Nakata *et al.*, 2011; Ando *et al.*, 2012; Ide, 2014]. The sizes and distributions of the patches determine how they interact and whether the dominant slip mode is fast or slow. Frictional models and laboratory observations also corroborate our interpretation [Leeman *et al.*, 2016]. Recent observations of the same portions of several plate boundary faults sometimes slipping slowly and other times fast enough to radiate significant seismic energy further imply that slip modes belong to a continuum governed by a single suite of physical processes [Veedu and Barbot, 2016].

Acknowledgments

Reviewers Thorne Lay, Takahiko Uchide, Satoshi Ide, Paul Segall, Barbara Romanowicz, Nick Beeler, David Schmidt, Chris Marone, Allan Rubin, and several anonymous reviewers provided helpful comments and suggestions. The authors also thank Nick Beeler and Noel Bartlow for their relevant insights shared in multiple exchanges. Data sources are described in the manuscript and supporting information.

References

- Aguilar, A. C., T. I. Melbourne, and C. W. Scrivner (2009), Moment release rate of Cascadia tremor constrained by GPS, *J. Geophys. Res.*, *114*, B00A05, doi:10.1029/2008JB005909.
- Aki, K. (1972), Earthquake mechanism, *Tectonophysics*, *13*, 423–446.
- Allmann, B. P., and P. M. Shearer (2009), Global variations of stress drop for moderate to large earthquakes, *J. Geophys. Res.*, *114*, B01310, doi:10.1029/2008JB005821.
- Ando, R., R. Nakata, and T. Hori (2010), A slip pulse model with fault heterogeneity for low-frequency earthquakes and tremor along plate interfaces, *Geophys. Res. Lett.*, *37*, L10310, doi:10.1029/2010GL043056.
- Ando, R., N. Takeda, and T. Yamashita (2012), Propagation dynamics of seismic and aseismic slip governed by fault heterogeneity and Newtonian rheology, *J. Geophys. Res.*, *117*, B11308, doi:10.1029/2012JB009532.
- Ben-Zion, Y. (2012), Episodic tremor and slip on a frictional interface with critical zero weakening in elastic solid, *Geophys. J. Int.*, *189*(2), 1159–1168, doi:10.1111/j.1365-246X.2012.05422.x.
- Bostock, M. G., A. M. Thomas, G. Savard, L. Chuang, and A. M. Rubin (2015), Magnitudes and moment-duration scaling of low-frequency earthquakes beneath southern Vancouver Island, *J. Geophys. Res. Solid Earth*, *120*, 1–22, doi:10.1002/(ISSN)2169-9356.
- Chapman, J. S., and T. I. Melbourne (2009), Future Cascadia megathrust rupture delineated by episodic tremor and slip, *Geophys. Res. Lett.*, *36*, L22301, doi:10.1029/2009GL040465.
- Colella, H. V., J. H. Dieterich, and K. Richards-Dinger (2013), Spatial and temporal patterns of simulated slow slip events on the Cascadia megathrust, *Geophys. Res. Lett.*, *40*, 5101–5107, doi:10.1002/grl.50984.
- Fletcher, J. B., and A. McGarr (2011), Moments, magnitudes, and radiated energies of non-volcanic tremor near Cholame, CA, from ground motion spectra at UPSAR, *Geophys. Res. Lett.*, *38*, L16314, doi:10.1029/2011GL048636.
- Gao, H., D. A. Schmidt, and R. J. Weldon (2012), Scaling relationships of source parameters for slow slip events, *Bull. Seismol. Soc. Am.*, *102*(1), 352–360, doi:10.1785/0120110096.
- Houston, H. (2001), Influence of depth, focal mechanism, and tectonic setting on the shape and duration of earthquake source time functions, *J. Geophys. Res.*, *106*, 11,137–11,150, doi:10.1029/2000JB900468.
- Houston, H., B. G. Delbridge, A. G. Wech, and K. C. Creager (2011), Rapid tremor reversals in Cascadia generated by a weakened plate interface, *Nat. Geosci.*, *4*(6), 404–409, doi:10.1038/ngeo1157.
- Ide, S. (2008), A Brownian walk model for slow earthquakes, *Geophys. Res. Lett.*, *35*, L17301, doi:10.1029/2008GL034821.
- Ide, S. (2014), Modeling fast and slow earthquakes at various scales, *Proc. Jpn. Acad. Ser. B*, *90*(8), 259–277, doi:10.2183/pjab.90.259.
- Ide, S., and S. Yabe (2014), Universality of slow earthquakes in the very low frequency band, *Geophys. Res. Lett.*, *41*, 2786–2793, doi:10.1002/(ISSN)1944-8007.
- Ide, S., G. C. Beroza, D. R. Shelly, and T. Uchide (2007), A scaling law for slow earthquakes, *Nature*, *447*(7140), 76–79, doi:10.1038/nature05780.
- Ide, S., K. Imanishi, Y. Yoshida, G. C. Beroza, and D. R. Shelly (2008), Bridging the gap between seismically and geodetically detected slow earthquakes, *Geophys. Res. Lett.*, *35*, L10305, doi:10.1029/2008GL034014.
- Ito, Y., K. Obara, K. Shiomi, S. Sekine, and H. Hirose (2007), Slow earthquakes coincident with episodic tremors and slow slip events, *Science*, *315*(5811), 503–506, doi:10.1126/science.1134454.
- Johnson, P. A., J. Carmeliet, H. M. Savage, M. Scuderi, B. M. Carpenter, R. A. Guyer, E. G. Daub, and C. Marone (2016), Dynamically triggered slip leading to sustained fault gouge weakening under laboratory shear conditions, *Geophys. Res. Lett.*, *43*, 1559–1565, doi:10.1002/(ISSN)1944-8007.
- Kanamori, H., and E. E. Brodsky (2004), The physics of earthquakes, *Rep. Prog. Phys.*, *67*(8), 1429–1496, doi:10.1088/0034-4885/67/8/R03.
- Kao, H., S.-J. Shan, H. Dragert, and G. Rogers (2009), Northern Cascadia episodic tremor and slip: A decade of tremor observations from 1997 to 2007, *J. Geophys. Res.*, *114*, B00A12, doi:10.1029/2008JB006046.
- Leeman, J. R., D. M. Saffer, M. M. Scuderi, and C. Marone (2016), Laboratory observations of slow earthquakes and the spectrum of tectonic fault slip modes, *Nat. Commun.*, *7*, 1–6, doi:10.1038/ncomms11104.
- Liu, Y. (2014), Source scaling relations and along-strike segmentation of slow slip events in a 3-D subduction fault model, *J. Geophys. Res. Solid Earth*, *119*, 6512–6533, doi:10.1002/(ISSN)2169-9356.
- Mai, P. M., and K. K. S. Thingbaijam (2014), SRCMOD: An online database of finite-fault rupture models, *Seismol. Res. Lett.*, *85*(6), 1348–1357, doi:10.1785/0220140077.

- Matsuzawa, T., K. Obara, and T. Maeda (2009), Source duration of deep very low frequency earthquakes in western Shikoku, Japan, *J. Geophys. Res.*, *114*, B00A11, doi:10.1029/2008JB006044.
- Nakata, R., R. Ando, T. Hori, and S. Ide (2011), Generation mechanism of slow earthquakes: Numerical analysis based on a dynamic model with brittle-ductile mixed fault heterogeneity, *J. Geophys. Res.*, *116*, B08308, doi:10.1029/2010JB008188.
- Obara, K. (2010), Phenomenology of deep slow earthquake family in southwest Japan: Spatiotemporal characteristics and segmentation, *J. Geophys. Res.*, *115*, B00A25, doi:10.1029/2008JB006048.
- Obara, K., S. Tanaka, T. Maeda, and T. Matsuzawa (2010), Depth-dependent activity of non-volcanic tremor in southwest Japan, *Geophys. Res. Lett.*, *37*, L13306, doi:10.1029/2010GL043679.
- Pacheco, J. F., C. H. Scholz, and L. R. Sykes (1992), Changes in frequency-size relationship from small to large earthquakes, *Nature*, *355*, 71–73.
- Peng, Z., and J. Gomberg (2010), An integrated perspective of the continuum between earthquakes and slow-slip phenomena, *Nature*, *3(9)*, 599–607, doi:10.1038/ngeo940.
- Romanowicz, B. (1994), Comment on "A reappraisal of large earthquake scaling", *Bull. Seismol. Soc. Am.*, *84*, 1675–1676.
- Schmidt, D. A., and H. Gao (2010), Source parameters and time-dependent slip distributions of slow slip events on the Cascadia subduction zone from 1998 to 2008, *J. Geophys. Res.*, *115*, B00A18, doi:10.1029/2008JB006045.
- Scholz, C. H. (1982), Scaling laws for large earthquakes: Consequences for physical models, *Bull. Seismol. Soc. Am.*, *72*(1), 1–14.
- Segall, P., A. M. Rubin, A. M. Bradley, and J. R. Rice (2010), Dilatant strengthening as a mechanism for slow slip events, *J. Geophys. Res.*, *115*, B12305, doi:10.1029/2010JB007449.
- Sekine, S., H. Hirose, and K. Obara (2010), Along-strike variations in short-term slow slip events in the southwest Japan subduction zone, *J. Geophys. Res.*, *115*, B00A27, doi:10.1029/2008JB006059.
- Shaw, B. E. (2013), Earthquake surface slip-length data is fit by constant stress drop and is useful for seismic hazard analysis, *Bull. Seismol. Soc. Am.*, *103*(2A), 876–893, doi:10.1785/0120110258.
- Shimazaki, K. (1986), in *Earthquake Source Mechanics, AGU Monogr.*, edited by S. Das, J. Boatwright, and C. Scholz, AGU, Washington D. C.
- Sugioka, H., T. Okamoto, T. Nakamura, Y. Ishihara, A. Ito, K. Obana, M. Kinoshita, K. Nakahigashi, M. Shinohara, and Y. Fukao (2012), Tsunamigenic potential of the shallow subduction plate boundary inferred from slow seismic slip, *Nat. Geosci.*, *5*(6), 414–418, doi:10.1038/ngeo1466.
- Tanioka, Y., and L. J. Ruff (1997), Source time functions, *Seismol. Res. Lett.*, *68*, 386–400.
- Uchide, T., and S. Ide (2010), Scaling of earthquake rupture growth in the Parkfield area: Self-similar growth and suppression by the finite seismogenic layer, *J. Geophys. Res.*, *115*, B11302, doi:10.1029/2009JB007122.
- Veedu, D. M., and S. Barbot (2016), The Parkfield tremors reveal slow and fast ruptures on the same asperity, *Nature*, *532*, 361–365, doi:10.1038/nature17190.
- Wech, A. G., K. C. Creager, H. Houston, and J. E. Vidale (2010), An earthquake-like magnitude-frequency distribution of slow slip in northern Cascadia, *Geophys. Res. Lett.*, *37*, L22310, doi:10.1029/2010GL044881.